

Effects of silt contents on the static and dynamic properties of sand-silt mixtures

Darn H. Hsiao^a and Vu T.A. Phan^{*}

*Department of Civil Engineering, National Kaohsiung University of Applied Sciences,
No. 415 Chien-Kung Road, Kaohsiung 80778, Taiwan R.O.C.*

(Received December 20, 2013, Revised May 30, 2014, Accepted June 05, 2014)

Abstract. This paper presents a detailed study focused on investigating the effects of silt content on the static and dynamic properties of sand-silt mixtures. Specimens with a low-plastic silt content of 0, 15, 30 and 50% by weight were tested in static triaxial, cyclic triaxial, and resonant columns in addition to consolidation tests to determine such parameters as compression index, internal friction angle, cohesion, cyclic stress ratio, maximum shear modulus, normalized shear modulus and damping ratio. The test procedures were performed on specimens of three cases: constant void ratio index, $e = 0.582$; same peak deviator stress of 290 kPa; and constant relative density, $D_r = 30\%$. The test results obtained for both the constant-void-ratio- index and constant-relative-density specimens showed that as silt content increased, the internal friction angle, cyclic stress ratio and maximum shear modulus decreased, but cohesion increased. In testing of the same deviator stress specimens, both cohesion and internal friction angle were insignificantly altered with the increase in silt content. In addition, as silt content increased, the maximum shear modulus increased. The cyclic stress ratio first decreased as silt content increased to reach the threshold silt content and increased thereafter with further increases in silt content. Furthermore, the damping ratio was investigated based on different silt contents in three types of specimens.

Keywords: sand-silt mixture; critical state parameter; cyclic stress ratio; shear modulus; damping ratio

1. Introduction

Located in Taiwan, Kaohsiung city is heavily influenced by natural hazards, e.g., earthquakes, typhoons, and landslides. In particular, Typhoon Morakot severely devastated Taiwan at midnight on the 7th of August 2009. A large land area collapsed, resulting in 619 deaths, 76 missing persons, temporary evacuation of 24,950 residents, flooding, and more than \$5 billion USD in damage to property (National Disasters Prevention and Protection Commission 2009). The Jiasian earthquake ($M_w = 6.4$) occurred on the 4th of March 2010 and was the biggest earthquake in Kaohsiung area since 1900. This seismic event caused many injuries, and many large buildings were damaged. Additionally, Typhoon Yinmolate caused extensive ground erosion in this area. In light of these events, it is therefore essential to understand the soil properties to perform accurate computations

*Corresponding author, Ph.D. Student, E-mail: phantoanhvu@yahoo.com

^a Associate Professor, Ph.D., E-mail: hsiaodh@cc.kuas.edu.tw

of the ground response and analyze the soil-structure interactions. In the past, considerable study efforts have focused on the static and dynamic properties of sandy soils. However, nearly all of this work has been directed towards either the static properties or dynamic properties, and no valuable data are available on both the static and dynamic properties in the survey area. The experimental work in this study was absolutely meaningful in providing valuable data for geotechnical design and structures in complicated geologic areas. Additionally, the relationships between the static and dynamic properties of sandy soil were investigated for the first time in Kaohsiung city, Taiwan in this work.

In general, natural sand commonly consists of fines and sand particles with different proportions, and the fines content significantly affects the engineering properties of sandy soil. Until recently, few studies have reported on the behavior of granular sandy and/or clayey soil with different fines contents.

Information on the static properties of sandy soil, the stress-strain relationship, and the shear strength behavior were the main concerns of previous researchers. Thevanayagam (1998) investigated the effects of non-plastic silt, intergranular void ratio, and initial confining stress on the undrained shear strength, and the results indicated that sand-silt containing greater than 30% silt exhibited the same behavior as silt. Thian and Lee (2011) revealed that the undrained shear strength, soil modulus, and pore pressure decreased when the clay content increased. Kim *et al.* (2005) performed a series of triaxial compression tests on soil mixed with various silt contents, and the results showed that the critical state friction decreased with the increase in fine aggregate content. Maleki *et al.* (2011) found that the undrained behavior of sand mixed with various non-plastic silt contents can be described using an equivalent void ratio that takes into account the non-plastic fine participation ratio in the soil-bearing skeleton. Belkhatir *et al.* (2013) determined the relationship between the undrained shear strength and the hydraulic conductivity of sand-silt mixtures and the void ratio of the soil. Other researchers reported that as silt content increased, the steady-state strength at the same void ratio initially decreased and subsequently increased in shear strength with further increases in the silt content to values greater than 30% (Zlatovic and Ishihara 1995, Thevanayagam *et al.* 1996).

With respect to the dynamic properties of sand-silt mixtures, the liquefaction resistance, cyclic stress ratio, shear modulus, and damping ratio have been commonly employed to evaluate the behavior of a material under foundational vibration or seismic excitation via earthquakes. A number of researchers have conducted in situ tests (Seed *et al.* 1983, Tokimatsu *et al.* 1994, Holzer *et al.* 2010, Cao *et al.* 2011). Numerous laboratory studies reported on various types of sand-silt mixtures and provided conflicted results. To evaluate the liquefaction, two sets of grain size curves showed the range of grain-size distribution for most liquefaction and liquefaction potentials of soils (Tsuchida 1970). However, based on the later experimental study of Ishihara *et al.* (1980) and Xenaki and Athanasopoulos (2003), use of the Tsuchida diagram is unsafe for soils with low plasticity to non-plasticity. Certain studies revealed that as the silt content increased, the liquefaction resistance either decreased (Vaid 1994, Yamamuro and Lade 1997, Lade and Yamamuro 1997) or increased (Amini and Qi 2000). Other researchers concluded that the liquefaction resistance decreased as the silt content increased until a limited silt content was reached but subsequently increased as the silt content continued to increase (Kuerbis *et al.* 1988, Koester 1994, Polito and Martin 2001). The remaining groups suggested that the liquefaction potential depends on the largest inter-granular void ratio and relative density (Xenaki and Athanasopoulos 2003, Belkhatir *et al.* 2010, 2013). Additionally, the shear modulus and damping ratio were investigated by selected researchers (Seed and Idriss 1970, Kokosho 1980, Chang *et al.*

1989, Orense *et al.* 2012).

In the current study, the static and dynamic properties of sand-silt mixtures were investigated using tests conducted in a laboratory. The test program employed static triaxial, cyclic triaxial and resonant column tests on various sand-silt mixtures with three types of specimens, i.e., a constant void ratio index of 0.582 (type A), the same peak deviator stress of 290 kPa with a confining pressure of 100 kPa (type B), and a constant relative density D_r of 30% (type C) to understand the effects of low-plastic silt content on the results of (a) the angle of internal friction and cohesion, (b) the liquefaction resistance, and (c) the shear modulus and damping ratio of sand-silt mixtures. This article presents one case as a component of a broader research effort on the properties of locally available soils for construction in the Liouguei area of Kaohsiung city, located in Taiwan. The experimental data provide a quantitative basis for further design recommendations in this area.

2. Materials used

A quantity of natural sandy soil was carefully sieved to separately obtain clean sand and pure silt. The silt particles are defined as the grain size of soil that is able to pass through a No. 200 (0.075 mm) sieve. The sand-silt mixtures were prepared from these two materials for the various following combinations.

All tests were conducted with four sand-silt mixtures defined by dry weight: 100% sand plus 0% silt (sample 1), 85% sand plus 15% silt (sample 2), 70% sand plus 30% silt (sample 3), and 50% sand plus 50% silt (sample 4). Based on the ASTM D422 method, the results of the grain size distribution curve for all of the sand-silt mixtures are shown in Fig. 1. The specific gravity test G_s was conducted in accordance with ASTM D854 and yielded a value of 2.7. It should be noted that no applicable ASTM procedure exists for determining the maximum void ratio over the entire range of silt content investigated. The ASTM 4254 method was limited to the determination of maximum void ratio with a maximum silt content of 15% in the mixture. Despite this limitation, the maximum void ratio was still tested according to this specification. Similar to the maximum void ratio, there was also no applicable ATSM procedure available for determining the minimum void ratio over the entire range of silt content investigated. The ASTM D4253 was limited to determination of the minimum void ratio with a maximum silt content of 15%. ASTM D4253 was

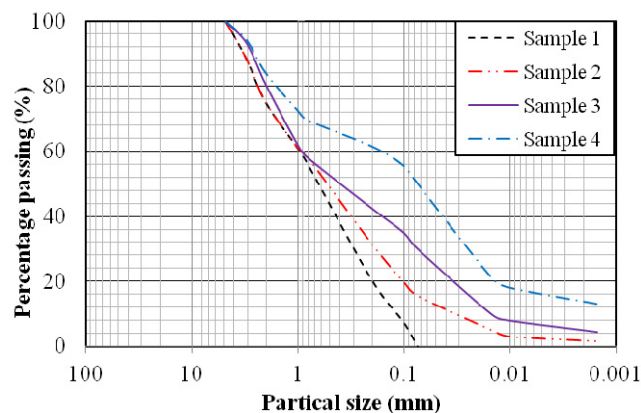


Fig. 1 Grain size distribution curves of the sand-silt mixtures

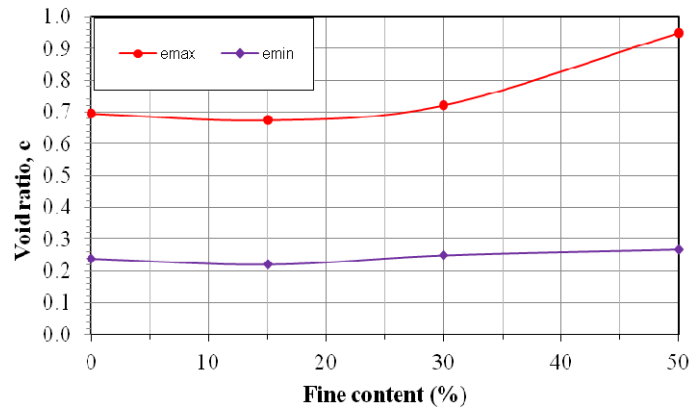


Fig. 2 Variation of the void ratio index with different silt contents in the sand-silt mixtures

Table 1 Basic physical properties of the sand-silt mixtures

Test	Sample 1	Sample 2	Sample 3	Sample 4
Effective size, D_{10} (mm)	0.12	0.032	0.015	-
Effective size, D_{30} (mm)	0.30	0.18	0.07	0.025
Effective size, D_{60} (mm)	0.95	0.90	0.89	0.16
Specific gravity, G_s	2.70	2.70	2.70	2.70
Minimum dry unit weight, γ_{dmin} (kN/m ³)	15.92	16.12	15.68	13.86
Maximum dry unit weight, γ_{dmax} (kN/m ³)	21.81	22.13	21.63	21.32
Maximum void ratio, e_{max}	0.696	0.675	0.722	0.948
Minimum void ratio, e_{min}	0.238	0.220	0.248	0.266
Uniformity coefficient, C_u	7.92	28.13	59.33	-
Coefficient of gradation, C_g	0.79	1.13	0.41	-
Liquid limit, LL (%)	-	17.93	20.83	26.24
Plastic index, PI (%)	-	3.12	5.04	6.73
Unified soil classification system, USCS	SP	SM	SC-SM	CL-ML

Table 2 Basic physical properties of sand mixtures in three types of specimens

Type	Sample 1			Sample 2			Sample 3			Sample 4		
	e	γ_d^*	D_r (%)	e	γ_d	D_r (%)	e	γ_d	D_r (%)	e	γ_d	D_r (%)
A	0.582	17.07	24.95	0.582	17.07	20.49	0.582	17.07	29.60	0.582	17.07	53.74
B	0.656	16.30	8.63	0.599	16.89	16.79	0.550	17.42	36.31	0.498	18.02	65.98
C	0.559	17.32	30	0.538	17.55	30	0.580	17.09	30	0.744	15.49	30

γ_d^* : dry unit weight (kN/m³)

used to test the maximum density to obtain the minimum void ratio index. The variation of void ratio index with changes in the silt content of the mixtures is expressed in Fig. 2. As shown in Fig. 2, both the maximum and minimum void ratio of sand-silt mixtures is initially reduced with an

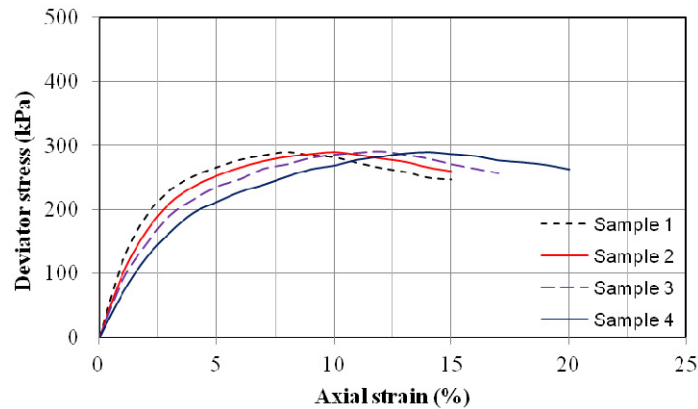


Fig. 3 Same peak deviator stress in the consolidated drained triaxial test

increase in silt content until it reaches a minimum value at a limited silt content of 18% and continuously increases with further increases in the silt content. The limit point was reached at 20% and 30% depending on the low- or non-plastic silt content (Koester 1994, Polito and Martin 2001). With a silt content less than this limited content, the structure was dominated by sand, and once this value was surpassed, the structure was converted to silt-dominated.

The basic physical properties of the sand-silt mixtures used in the laboratory are listed Table 1. It is clear that the silts consist of low-plastic particles that can be discerned by the liquid limit (LL) and plastic index (PI). According to the Unified Soil Classification System (USCS), the classification of sand-silt mixtures with silt contents (FC) of 0, 15, 30 and 50% are graded as poor sand (SP), silty sand (SM), silty clayey sand (SC-SM), and silty clay with sand (CL-ML), respectively.

All of the tests were carried out on the specimens with various silt contents (FC), i.e., 0, 15, 30, and 50% by weight corresponding to the three types of specimens. Type A was conducted on specimen with same void ratio of 0.582. Type B was carried out on specimens that had the same peak deviator stress of 290 kPa when tested in the triaxial test. To obtain the same peak deviator stress of 290 kPa, a series of samples 1 to 4 was gradually constructed with various void ratios as well as dry unit weights, and thereafter, each sample was tested on consolidated drained triaxial shear test with a confining pressure of 100 kPa to obtain the peak deviator stress. Selected specimens had a peak deviator stress of 290 kPa, as shown in Fig. 3. Type C was performed on specimens with a constant relative density of 30%. The relative density is calculated as a function that depends on void ratio of the specimen and the maximum and minimum index void ratios for each sand-silt mixture. The basic physical properties for three types of specimens are also listed in Table 2.

3. Sample preparation and tests

The experimental test program can be divided into three components. the first aim is to determine the angle of internal friction and cohesion, the second aim is to determine the cyclic stress ratio, and the third aim is to determine the maximum shear modulus, normalized shear modulus and damping ratio. Moreover, certain basic tests are also conducted in this study.

The diameter and height of the specimens were 7.1 cm and 15 cm, respectively, for static and cyclic triaxial testing and resonant column testing. The specimens were prepared using the wet tamping method. For sample preparation, dry sand and silt were mixed in the selected weight ratio. The dry mixture was first divided into five equal parts. To each part was added an amount of de-aired water and mixed into the wet mixture with an exact water content of 8%. Next, each part was set up in a mold covered by a rubber membrane and compacted to a given height. Finally, to make a good contact between the layers, the surface of each tamping layer was roughened to a depth of 5 mm using a knife. The same initial dry densities were maintained during test preparation.

The specimen was subsequently saturated with flowing carbon dioxide CO₂ for at least 30 minutes, and thereafter, de-aired water was allowed to flow through the specimen from the bottom to the top to ensure that the Skempton's coefficient B was 0.95 or greater at the end of the saturation process. In this study, a backpressure of 200 kPa was applied during the test to reach the saturation state. A confining pressure was applied to the specimens for the consolidation stage. During consolidation, the difference between the confining pressure and backpressure was set up such that the effective consolidation pressure was fixed at 100 kPa for each sample.

Static triaxial testing was conducted in the consolidated-drained and consolidated-undrained stage, and the apparatus is shown in Fig. 4. The test procedure used a static triaxial testing device (manufactured by ELE Co., United Kingdom) that was automatically controlled using hydraulic lifting equipment and collected measured data with a digital display monitor. Confining pressures of 50, 100, and 200 kPa were applied in all tests.

The cyclic triaxial tests were conducted in accordance with ASTM D5311 using the automatic triaxial testing system, as shown in Fig. 5. This testing equipment was fabricated by the Soil Equipment Company, San Francisco, California; namely CKC cyclic triaxial device. During cyclic axial loading, a sinusoidal load was applied to the saturated specimens. The variations in excess pore water pressure, axial stress, and axial strain of the specimens were recorded during cyclic loading. The frequency of cyclic loading was fixed at 1 Hz. The results were characterized in terms of cyclic stress ratio (CSR), defined as the peak shear stress ($\sigma_d/2$) divided by the initial effective consolidation stress σ'_c . A series of cyclic triaxial tests were conducted on various sand-silt mixtures with silt contents from 0 to 50% at a 100-kPa effective confining pressure to determine the liquefaction resistance.

The resonant column apparatus was manufactured by Structural Behavior Engineering Laboratory Inc. and is also known as the Stokoe torsional shear/resonant column device, as shown



Fig. 4 Static triaxial test



Fig. 5 Dynamic triaxial test

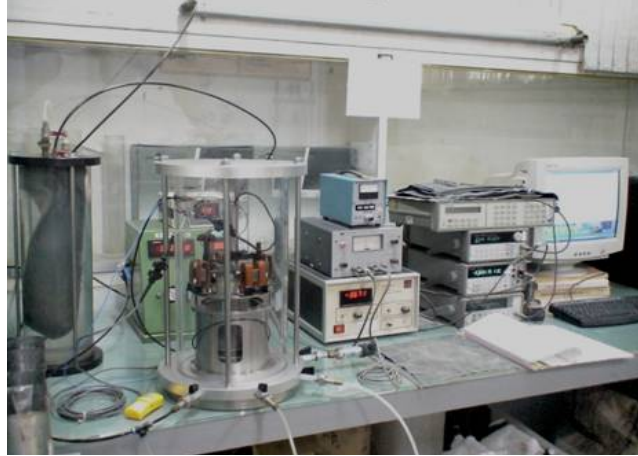
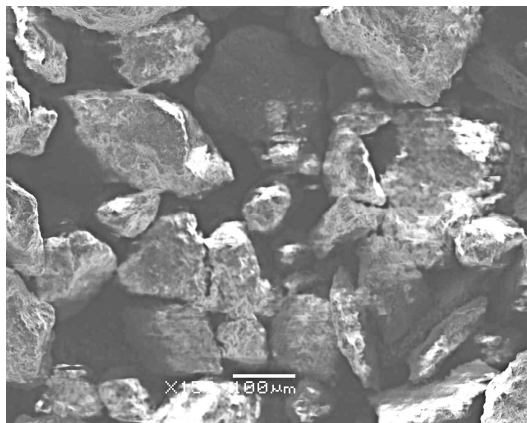
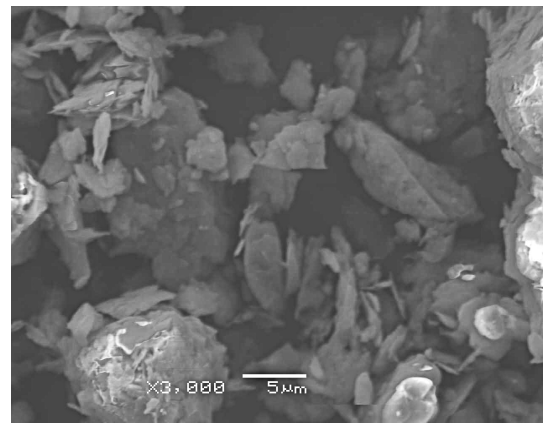


Fig. 6 Resonant column test



(a) Clean sand, magnified 150 times



(b) Silt, magnified 3,000 times

Fig. 7 Images of clean sand and silt

in Fig. 6. The measurements for shear modulus and damping ratio were obtained using the resonant column test conducted according to ASTM D4015. The device is a fixed-free system consisting of a cylindrical specimen with platens attached to each end. During the resonant column test, a sinusoidal vibration excitation device with a frequency from 2 Hz to 60 Hz is applied to the top of specimen. The above testing description corresponds to a cyclic torque of constant amplitude and varying frequency applied to the top of the specimen. Variations of the peak torsional displacements were recorded with changes in frequency, and the frequency response curve was constructed. The resonant frequency corresponding to the peak of the curve was noted. The dynamic soil properties, e.g., shear small-strain, shear modulus G and damping ratio D , can be obtained from the relationship between the resonant frequency and frequency response curve. To investigate the strain range, three levels of confining pressure of 50, 100 and 200 kPa were applied on each specimen.

4. Test results and discussions

4.1 Natural particles of material

The Scanning Electron Microscope (SEM) technique was employed to investigate the shape and surface of the natural particles of clean sand and silt. The results are shown in Figs. 7(a) and (b), and the clean sand and silt were magnified 150 and 3,000 times, respectively. Fig. 7(a) shows that the grains of clean sand included different sizes and a highly porous structure. The predominant particle shapes were mainly angular, sub-angular, or sub-rounded depending on the sharpness of the edges and corners of each particle. Additionally, the silt particles were observed to contain fewer shapes under a single particle, i.e., cylindrical, ellipsoidal and tabular, and clusters of smaller particles, as shown in Fig. 7(b). Preliminary assessment indicates that the structure of silt is likely to be weaker than that of clean sand.

4.2 Compression characteristics

The one-dimensional consolidation test was performed to determine the compression index C_c , which is also a key parameter in the design of engineering structures and evaluation of their performance. The three cases considered during testing were conducted with pressures of 25, 50, 100, 200, 400, 800 and 1600 kPa.

Fig. 8 shows the compression index C_c obtained from the one-dimensional consolidation test. The results from type A reveal that as the silt content increases, the compression index increases, and the behavior of the material mixture is similar to that of loose sand. This result is in agreement with the previous study (Kim *et al.* 2005). The result from type B showed that as the silt content increases, C_c increases to a peak compression index of 0.145 associated with a silt content of 20%, and thereafter, C_c decreases with further increases in silt content. This phenomenon of type B was thought to be tied to a silt content smaller than 20%, and although the higher relative density was obtained with the higher silt content, the structure was still dominated by sand, and the low plasticity of the higher silt content allowed the sand particles to easily move around each other during the loading process. Hence, the sand-silt mixture behaved similarly to loose sand. In contrast, for silt contents greater than 20%, the structure was mostly dominated by silt particles. In

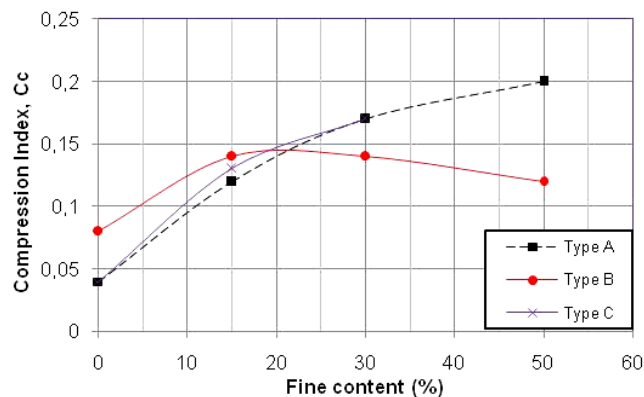


Fig. 8 Compression index with various silt contents for types A, B, and C

fact, as shown in Table 2, the relative density increased remarkably with the increase in silt content, and the stiffness of the mixture was supported by the low plasticity silt; therefore, the mixture behaved as a dense sand. Similar to type A, the result of type C also expresses an increasing tendency in C_c with the increase in silt content.

4.3 Results of static triaxial tests

Fig. 9 presents the variation of the shear envelopes with different silt contents and with respect to the three cases of specimens considered in this study. The detailed results of consolidated drained (CD) and consolidated undrained (CU) triaxial test (i.e., cohesion (c), internal friction angle (ϕ), and critical state parameter (M)) are listed in Tables 3-4. It is interesting to note that the cohesion obtained in the CD and CU tests are line-fitting parameters. For example, sample 1 represents clean sand and a cohesionless soil, and based on the principle of Coulomb theory, it should have a cohesion c equal to 0.

To investigate the relationship between static and dynamic properties of silty sand, the type A test was investigated in both consolidated drained and consolidated undrained triaxial shear testing. The results indicate that the shear parameters are significantly influenced by the silt content and testing conditions. For the consolidated drained test, the greater the silt content in the sand-silt mixture, the smaller the angle of internal friction becomes, and thus the cohesion is greater. The

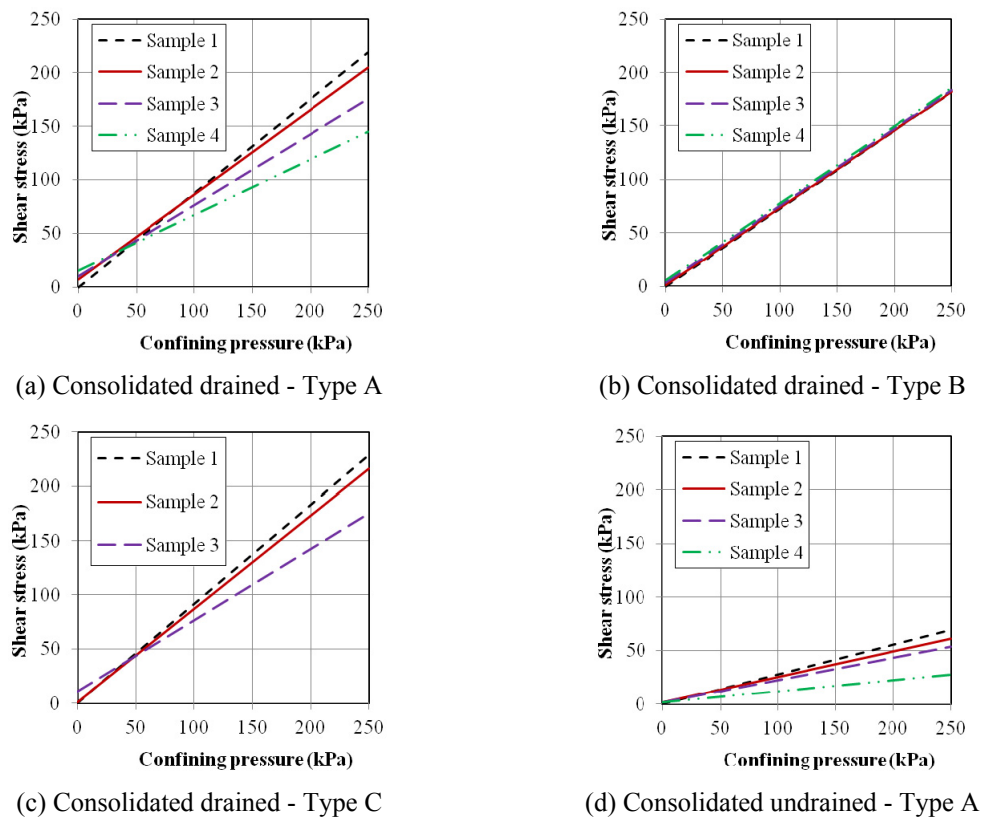


Fig. 9 Shear stress versus confining pressure in the test

main reason for this observation is that in the drained shear environment, the low-plastic silt particles not only mobilize the cohesive strength but also take advantage of the slipping between aggregate particles. In contrast, as the silt content increases, both the cohesion and internal friction angle decrease when the consolidated undrained triaxial test is conducted on type A. These behaviors most likely occur because the low-plastic particles are difficult to mobilize the cohesive strength in the mixture with the presence of pore water pressure; moreover, the low-plastic particles also contribute to the easy slip between the aggregate particles in the undrained shear environment.

Fig. 10 shows the relationships of deviator stress, volumetric strain, and pore water pressure (PWP) versus axial strain in the consolidated drained and consolidated undrained triaxial tests with type A. Other specimens are included due to the same tendency. It is clear from Fig. 10(a) that as the silt content increases, the peak deviator stress is decreased corresponding to the axial strain range of 12% and 17%. Furthermore, it is noted that an increase in the amount of silt particles requires a longer time duration to reach the same deviator stress, and the volumetric strain decreases with the increase in silt content. These behaviors most likely occur because as the sand-silt mixture includes additional silt particles, the friction of the mixture remarkably decreases in the consolidated drained shear test. Fig. 10(b) shows that the deviator stresses quickly reach the peak value with an axial strain in the range of 0.5 and 2%, and thereafter, drop significantly in value with the increase in axial strain. As shown in Fig. 10(b), the pore water pressure (PWP) of all sand-silt mixtures rapidly increases as the axial strain reaches 1-2%, and afterward, the PWP slowly increases and reaches a stable state with a strain of 5% and 6%; however, the PWP of clean sand increases more slowly than that of the sand-silt mixtures.

The critical state parameter (M) is also known as the slope of the deviator stress and mean strain. The behaviors of the soils are substantially affected by the critical state parameter, which can be obtained from the following equation (Wood 1991)

$$M = \frac{6 \sin \phi}{3 - \sin \phi} \quad (1)$$

where ϕ is the angle of internal friction.

To more clearly understand the critical state parameter, Fig. 11 expresses the M value of two samples, i.e., sample 1 and sample 4, in the consolidated drained and consolidated undrained tests. The results listed in Tables 3-4 combined with those of Fig. 10 demonstrate that the M value decreases with the increase in silt content. As shown in Figs. 11(c) and (d), the stress path increases to reach the peak value and continues to move towards the bottom left, which is not

Table 3 Test results in the consolidated drained triaxial shear test

Type	Sample 1			Sample 2			Sample 3			Sample 4		
	c' (kPa)	ϕ' (°)	M									
A	0	41.21	1.69	6.8	38.38	1.57	10.3	33.43	1.35	15.3	27.38	1.09
B	0	36.10	1.47	1.4	35.90	1.44	3.6	35.82	1.45	5.8	35.75	1.45
C	0	42.47	1.74	1.3	40.63	1.66	10.3	33.42	1.35	-*	-*	-*

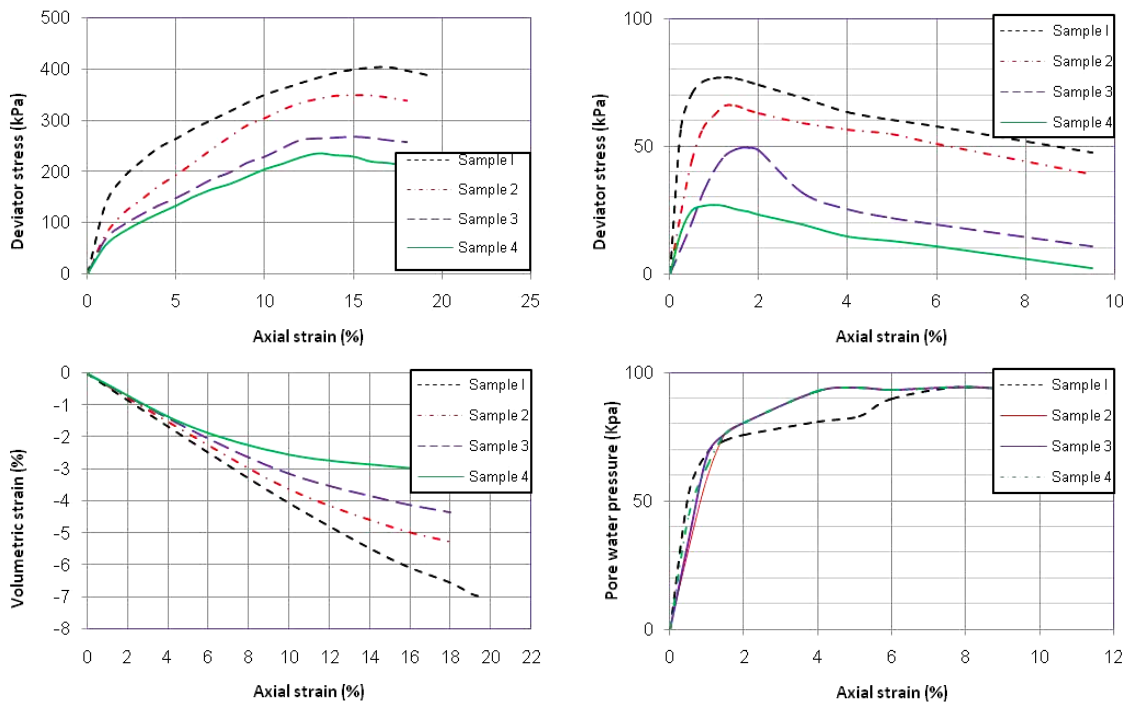
* -: Results were not obtained due to weak sample

* c' : effective cohesion; ϕ' : effective friction angle

Table 4 Test results in the consolidated undrained triaxial shear test

Type	Sample 1			Sample 2			Sample 3			Sample 4		
	c_u (kPa)	ϕ_u (°)	M									
A	0	15.48	0.59	1.9	13.37	0.52	1.6	11.67	0.43	1.5	5.99	0.22

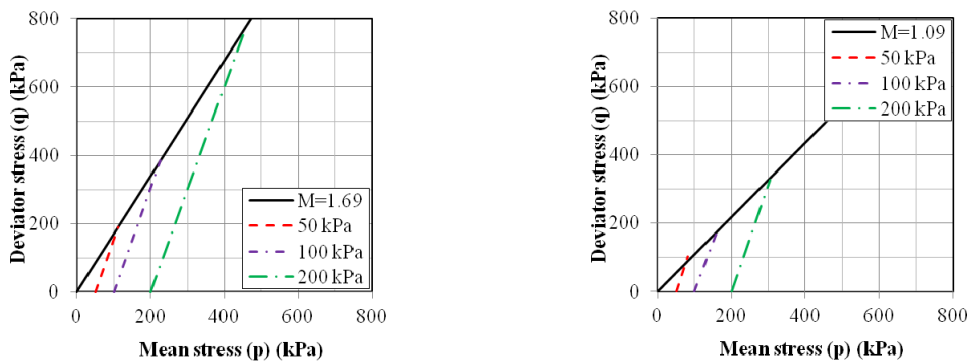
c_u : total cohesion; ϕ_u : total friction angle



(a) Consolidated drained - Type A

(b) Consolidated undrained – Type A

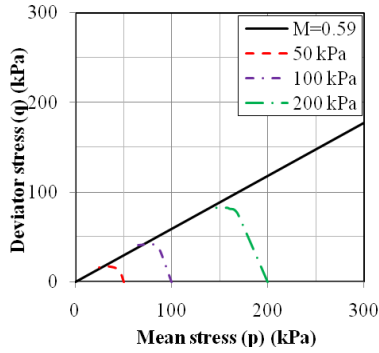
Fig. 10 (a) Deviator stress and volume change; (b) Deviator stress and pore water pressure at a confining pressure of 100 kPa



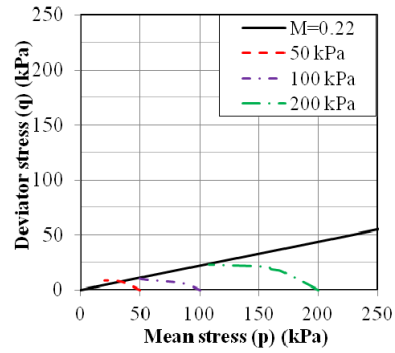
(a) Type A – consolidated drained, sample 1

(b) Type A – consolidated drained, sample 4

Fig. 11 Critical state parameter for different type of soils

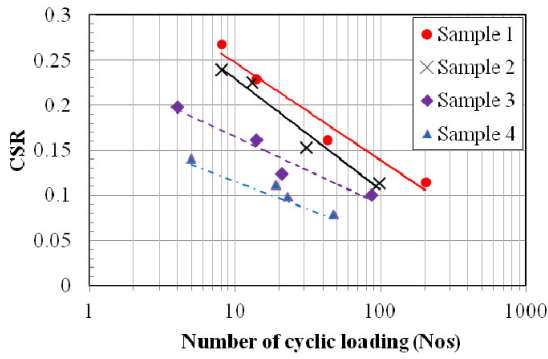


(c) Type A – consolidated undrained, sample 1

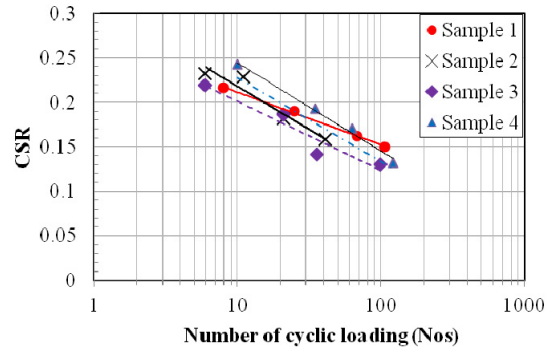


(d) Type A – consolidated undrained, sample 4

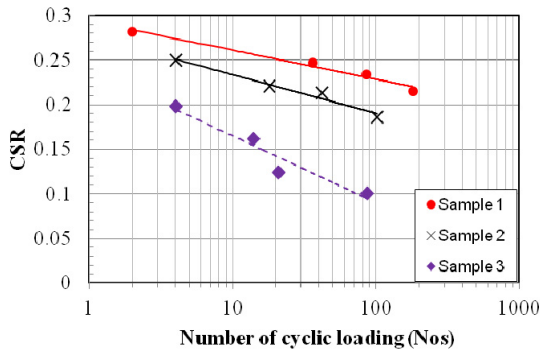
Fig. 11 Continued



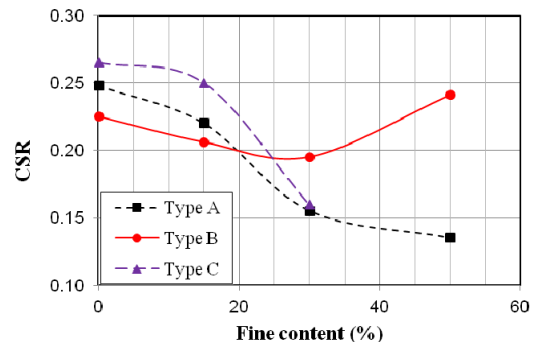
(a) Type A



(b) Type B



(c) Type C



(d) Cyclic stress ratio versus silt content

Fig. 12 Cyclic stress ratio

observed in Figs. 11 (a)-(b). The main reason for this observation is that in the consolidated undrained test, soil particles are not able to sustain the high deviator stress in the high pore water pressure condition, and the obtained result is a declining stress path tendency before reaching the failure stage.

4.4 Results of cyclic triaxial tests

The cyclic triaxial test was conducted on various sand-silt mixtures with three types of specimens, i.e., type A, type B, and type C, and the effect of substituting silt content in the cyclic stress ratio of the mixture was observed. Figs. 12(a)-(c) summarize the results of the cyclic stress ratio (CSR) according to the number of cyclic loadings. To estimate the liquefaction resistance of specimens with an earthquake of magnitude 7.5, the liquefaction resistance is defined as the cyclic stress ratio required to cause initial liquefaction within 15 cycles of loading.

The variation of the cyclic stress ratios with different silt contents are summarized in Fig. 12(d). It is obvious that with testing of type A, the greater the silt content in the mixture, the smaller the CSR obtained. The CSR of clean sand was approximately 1.13, 1.54, and 1.84 times larger than that of mixtures containing silt contents of 15, 30 and 50%, respectively. The increasing tendency in this result was in agreement with selected previous studies (Zlatovic and Ishihara 1997, Bekhatir *et al.* 2010).

The cyclic stress ratio was evaluated with tests on type C. As clearly shown in Fig. 12(d), the CSR gradually decreases with the increase in silt content from 0% to 15%, and afterwards, the value significantly decreases with further increases in silt content to 30%. The result from the specimen with 50% silt content was not obtained due to a weak sample.

Based on the results of type B, Fig. 12(d) also shows that increases in the silt content will decrease the CSR of the sand-silt mixture until the silt content approaches the limit value of 30%. Furthermore, as the silt content increases to greater than 30%, the CSR increases. Thevanayagam (1998) and Polito and Martin (1999) also reported that a similar trend was achieved using a specimen with constant void ratio testing.

The relationship between the angle of internal friction and the CSR of the sand-silt mixture is described in Fig. 13. The evidence reveals that with an increase in the internal friction angle in the sand-silt mixture, the cyclic stress ratio generally increases. However, in type B testing, the cyclic stress ratio depends not only on the friction internal angle but also on the silt content in the mixture; for the same internal friction angle in the sand-silt mixtures, the cyclic stress ratios are different. The test results contribute to an understanding of the relationship between the static and dynamic properties of sandy soil containing different silt contents in the study area.

4.5 Results of resonant column tests

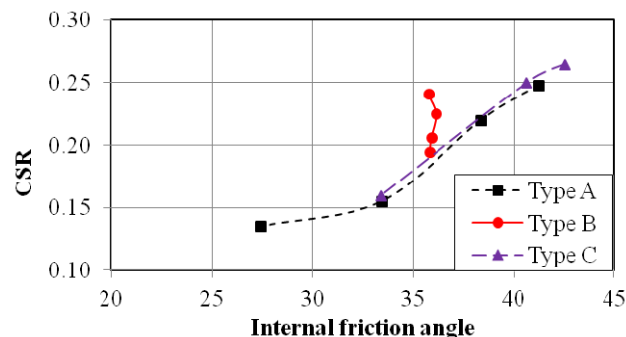


Fig. 13 Relationship between internal friction angle and CSR

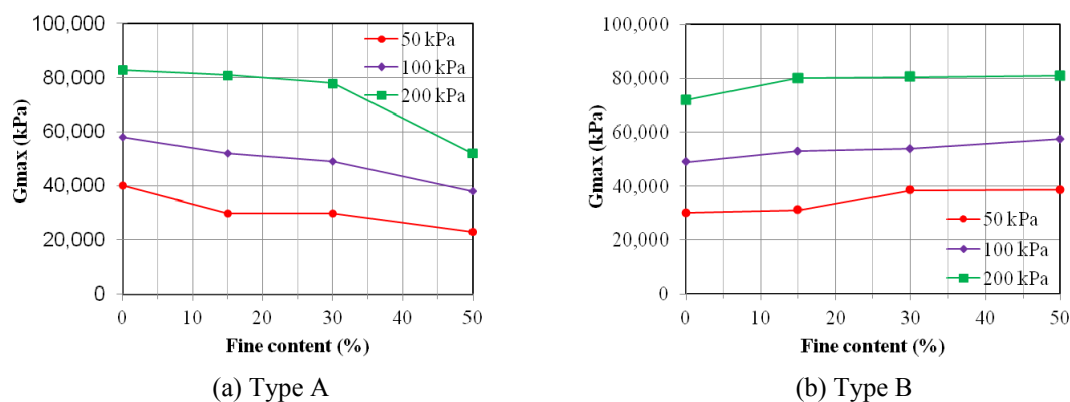


Fig. 14 Variation of maximum shear modulus versus silt content

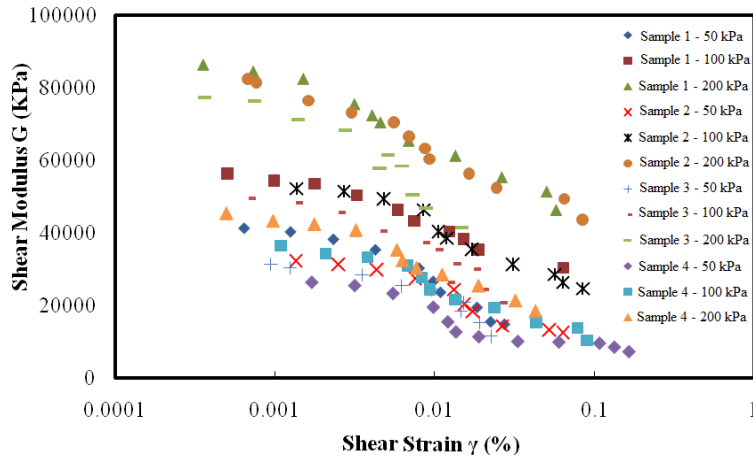
A series of resonant column tests were conducted on various sand-silt mixtures with silt contents of 0, 15, 30 and 50% for type A, type B, and type C. The specimens were subjected to confining pressures of 50 kPa, 100 kPa, and 200 kPa. The test results from type C produced the same tendency as type A and are thus not shown. Fig. 14 clearly shows the results of testing the maximum shear modulus G_{\max} versus silt content, which was conducted on type A and type B. The general tendency presented in Figs. 14(a) and (b) indicates that the maximum shear modulus is considerably influenced by both silt content and confining pressure.

For type A, Fig. 14(a) shows that the maximum shear modulus decreases with the increase in silt content, and a smaller maximum shear modulus is obtained with greater silt content in the mixture. The results are in agreement with the observation made by Orense *et al.* (2012). The decreasing tendency of G_{\max} is quite pronounced as the silt content exceeds 30%. In addition, the value of G_{\max} increases with the increase in confining pressure, and the increment of the maximum shear modulus between confining pressures of 200 and 100 kPa is much higher than that between 100 and 50 kPa. With a confining pressure of 100 kPa, the maximum shear modulus values of mixtures with silt contents of 15, 30 and 50% are approximately 0.92, 0.88 and 0.64 times smaller than that of clean sand, respectively. The reason for this observation may be that the stiffness of clean sand is greater than that of the sand-silt mixture, and with the greater silt content in the mixture, the role of coarse grain begins to diminish and leads to a decrease in the maximum shear modulus.

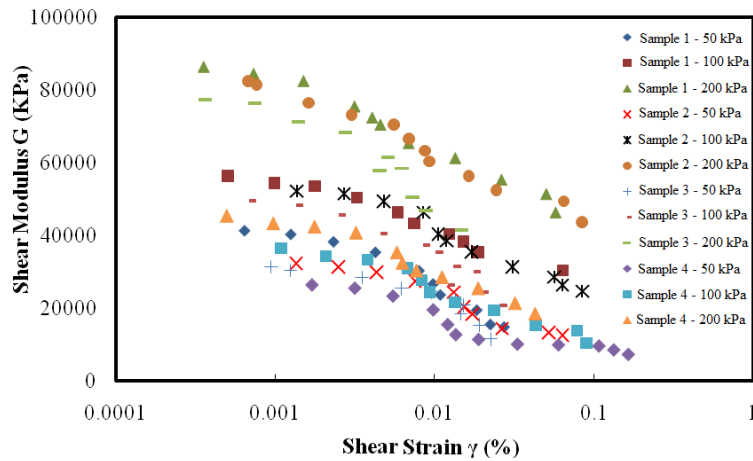
Similarly, Fig. 14(b) presents the results of testing of the maximum shear modulus versus silt content of type B. The maximum shear modulus also increases with the increase in confining pressure. However, G_{\max} slightly increases with the increase in the silt content, but the tendency is unclear for silt contents much greater than 30%. This observation is most likely explained by the use of the void ratio index of mixtures. For type B, when the silt content increases, the void ratio index of the specimen decreases, the elastic stiffness of the specimen increases, and a larger maximum shear modulus is obtained.

The relationships between the shear modulus and the amplitude of shear strain are shown in Figs. 15(a)-(b). It is well known that the deformation characteristics of sandy soils are highly nonlinear. Therefore, the shear modulus varies significantly with the amplitude of the shear strain under cyclic loading.

In general, Fig. 15(a) shows that the shear modulus increases with the increase in confining



(a) Type A



(b) Type B

Fig. 15 Shear modulus versus shear strain

pressure and also decreases with the increase in silt content because the specimens of type A were tested with the same void ratio; thus, clean sand expresses stiffer elastic behavior compared with that of the sand mixed with silt content at the same amplitude of shear strain, and the shear modulus is therefore higher. Furthermore, the shear modulus decreases with the increase in the amplitude of shear strain; however, the rate of reduction in the shear modulus with the amplitude of shear strain increases as the confining stress decreases.

In contrast, Fig. 15(b) shows that the shear modulus increases with the increase in silt content when specimens are subjected to a confining pressure of 100 kPa and 200 kPa. However, this trend is unclear with a confining pressure of 50 kPa. For instance, at a confining pressure of 50 kPa, the shear modulus of sample 4 is greater than that of sample 3, and the value for sample 3 is greater than that of sample 2, but the value of sample 2 is smaller than that of sample 1. It is thought that with a low confining pressure of 50 kPa, the mixture with 15% silt content still expresses a smaller

stiffness behavior than clean sand even though its relative density is slightly higher.

It is common to present the variation of shear modulus at any amplitude of shear strain level by normalizing it with the maximum shear modulus. Figs. 16(a) and (b) present the variation of the normalized shear modulus versus strain at different silt content of 0, 15, 30 and 50% with confining pressures of 50, 100, and 200 kPa, respectively, for type A and type B. Based on the normalized shear modulus, the G/G_{\max} , effects of different factors on the shear modulus of sandy soil can be observed.

For type A, Fig. 16(a) indicates that the normalized shear modulus responds elastically at an amplitude of shear strain that is less than 0.002%. It is clear that a small degradation of the normalized shear modulus occurs with an amplitude of shear strain that is less than 0.002%. Hence, the degradation of the dynamic shear strength and the post-cyclic shear strength would be insignificant in this range of amplitude of shear strain. However, once this limited shear strain is exceeded and the amplitude of shear strain reaches 0.02%, the normalized shear modulus expands the range of values and remarkably decreases with the further increases in the amplitude of shear

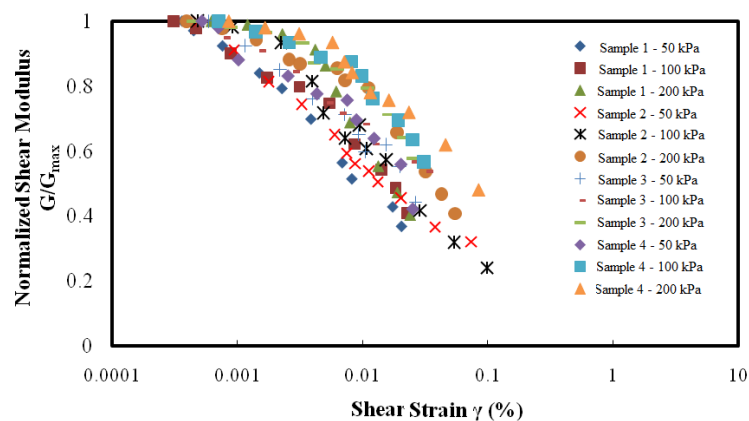
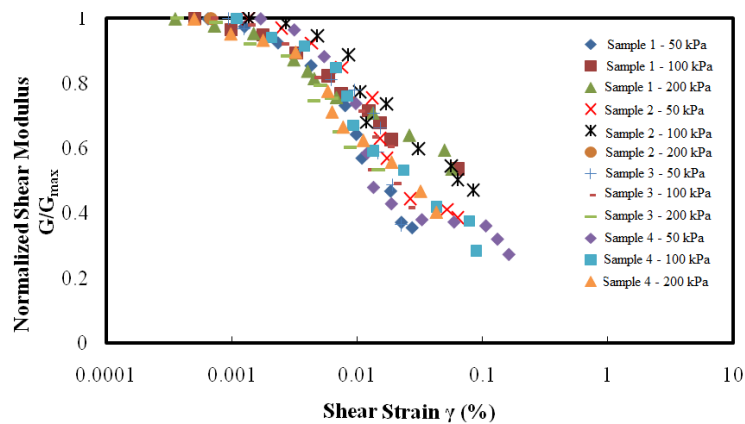
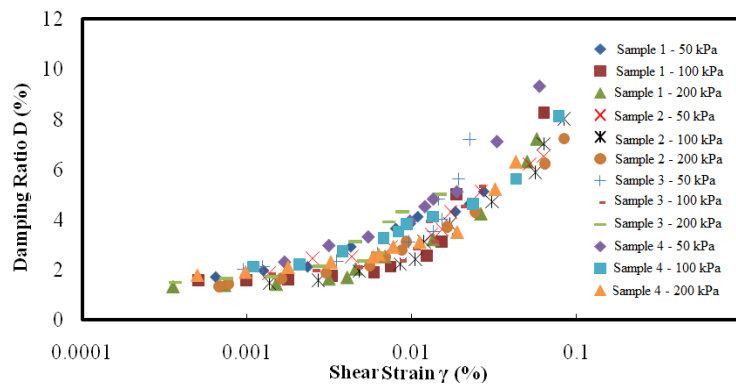


Fig. 16 Normalized shear modulus versus shear strain

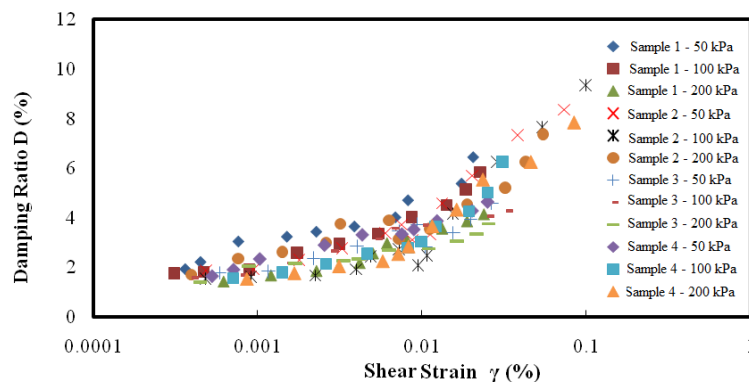
strain. In this stage, the shear modulus remarkably shrinks due to strain softening, breakdown of the particle structure, and pore water pressure build-up. With a shear strain greater than 0.02%, the degradation of the shear modulus is insignificant. A similar trend was also obtained by Okur and Ansal (2007), who conducted tests on fine-grained soil with a different plastic index.

In the same way, Fig. 16(b) shows that the normalized shear modulus considerably decreases with the increase in shear strain. Once the amplitude of the shear strain increases, the normalized shear modulus significantly decreases and expands the range of its value. In particular, sample 4 describes a significant increasing tendency in the normalized shear modulus with a confining pressure of 100 and 200 kPa. Comparing the results of Figs. 16(a) and (b), type A and type B show different degradations of the normalized shear modulus with the amplitude of shear strain, and the normalized shear modulus of type A is greater than that of type B at the same amplitude of shear strain. In comparison with the previous study, the results of the normalized shear modulus generally coincide with the observations of Seed and Idriss (1970).

Finally, the relationship between the damping ratio D and shear strain amplitude γ is described in Figs. 17(a)-(b). For shear strains less than 0.01%, the damping ratio slowly increases with the shear strain and significantly increases with greater shear strain. Furthermore, the damping ratio slightly decreased as the confining pressure increases. This observation can be explained in the



(a) Type A



(b) Type B

Fig. 17 Damping ratio versus shear strain

following manner: as the confining pressure increases, the specimens become more consolidated, and it is quite difficult to dissipate the energy during seismic dynamic loading.

Fig. 17(a) shows that the samples with greater amounts of silt generally have larger damping ratios; however, the difference between the silt contents is minimal. However, Fig. 17(b) indicates that the damping ratio decreases with the increase in silt content. As shown in Table 2, the decrease in the damping ratio of type B can be explained in the following manner: as the silt content increases, both the dry unit weight and relative density increase, which means that the stiffness of the specimen is significantly increased, and therefore, the damping ratio is decreased. Generally, the damping ratios obtained from these results are in notably good agreement with the observations made by Chang *et al.* (1989).

5. Conclusions

The effects of silt content on the static and dynamic properties of sand-silt mixtures were investigated in the current laboratory study. Based on the obtained results, the following conclusions were drawn:

- The maximum and minimum void ratio reached minimum values with silt contents of 18% in the sand-silt mixture.
- The one-dimensional consolidation test indicated that the behaviors of the material mixtures were similar to those of loose sand when the testing was conducted on constant-void-ratio and constant-relative-density specimens. However, with the same-peak-deviator-stress specimens, the behaviors of the material mixtures were similar to those of either loose sand or dense sand based on a silt content greater or smaller than 20%.
- For the consolidated drained shear test, as the silt content increased, all parameters of deviator stress, volumetric strain, shear stress, internal friction angle, and cohesion increased. The critical state parameter (M) decreased for constant-void-ratio and constant-relative-density specimens and seemed stable with the same-peak-deviator-stress specimens. Moreover, as the silt content increased, type A also showed degradation in the cohesion, internal friction angle, and critical state in the consolidated undrained shear test.
- The cyclic stress ratio decreased with an increase in silt content in testing with constant-void-ratio and constant-relative-density specimens. However, with the same-peak-deviator-stress specimens, as the silt content increased, the CSR of sand-silt mixture decreased until the silt content reached the limit content of approximately 30%, and thereafter, the CSR increased with further increases in the silt content.
- Both the maximum shear modulus and shear modulus decreased with the increase in silt content for constant-void-ratio and constant-relative-density specimens, but a reverse trend was obtained with testing of the same-peak-deviator-stress specimens. The normalized shear modulus obtained by testing with constant-void-ratio specimens was greater than that of the same-peak-deviator stress specimens at the same shear strain.
- For increasing silt content, the damping ratio increased in testing on constant-void-ratio and constant-relative-density specimens. However, with testing on the same-peak-deviator-stress specimens, the damping ratio decreased with increases in silt content, and the damping ratio was primarily dependent on the amplitude of shear strain.

Acknowledgments

The experimental work was carried out at the Department of Civil Engineering at KUAS, Taiwan. The authors thank Mr. Hsin-Yi Kuo for providing helpful data.

References

- Amini, F. and Qi, G.Z. (2000), "Liquefaction testing of stratified silty sands", *J. Geotech. Geoenviron. Eng., ASCE*, **126**(3), 208-217.
- Belkhatir, M., Arab, A., Della, N., Missoum, H. and Schanz, T. (2010), "Liquefaction resistance of Chlef river silty sand: effect of low plastic fines and other parameter", *Acta Polytechnica Hungarica*, **7**(2), 119-137.
- Belkhatir, M., Schanz, T. and Arab, A. (2013), "Effect of fines content and void ratio on the saturated hydraulic conductivity and undrained shear strength of sand-silt mixtures", *Environ. Earth Sci.*, **70**(6), 2469-2479.
- Cao, Z., Youd, T.L. and Yuan, X. (2011), "Gravelly soils that liquefied during 2008 Wenchuan, Chiana earthquake, $M_s = 8.0$ ", *Soil Dyn. Earthq. Eng.*, **31**(8), 1132-1143.
- Chang, T.S., Hwang, H. and Ng, K.W. (1989), "Subsurface conditions in memphis and shelby country", Tennessee. NCEER-89-0021, Buffalo, NY, USA.
- Holzer, T., Jayko, A.S., Hauksson, E., Fletcher, J.P.B., Noce, T.E., Bennett, M.J., Dietel, C.M. and Hudnut, K.W. (2010), "Liquefaction caused by the 2009 Olancha, California (USA), M5.2 earthquake", *Eng. Geol.*, **116**(1), 184-188.
- Ishihara, K., Troncoso, J., Kawase, Y. and Takahashi, Y. (1980), "Cyclic strength characteristics of tailings materials", *Soil. Found.*, **20**(4), 127-142.
- Kim, D., Sagong, M. and Lee, Y. (2005), "Effects of aggregate content on the mechanical properties of the compacted decomposed granitic soils", *Construct. Build. Mater.*, **19**(3), 189-196.
- Koester, J.P. (1994), "The influence of fines type and content on cyclic strength", *Ground Fail. Under Seismic Condit.*, ASCE, New York, USA, pp. 17-33.
- Kokusho, T. (1980), "Cyclic triaxial test of dynamic soil properties for wide strain range", *Soil. Found.*, **20**(2), 45-60.
- Kuerbis, R., Nigussey, D. and Vail, Y.P. (1988), "Effect of gradation and fines content on undrained response of sand", *Hydra. Fill Struct.*, ASCE, New York, 330-345.
- Lade, P.V. and Yamamuro, J.A. (1997), "Effects of nonplastic fines on static liquefaction sands", *Can. Geotech. J.*, **34**(6), 918-928.
- Maleki, M., Ezzatkhah, A., Bayat, M. and Mousivand, M. (2011), "Effect of physical parameters on static undrained resistance of sandy soil with low silt content", *Soil Dyn. Earthq. Eng.*, **31**(10), 1324-1331.
- National Disasters Prevention and Protection Commission (2009). [In Taiwan]
- Orense, R.P., Hyodo, M. and Kaneko, T. (2012), "Dynamic deformation characteristics of pumice", *2012 NZSEE Annual Technical Conference*, Christchurch, New Zealand, April, pp. 1-8.
- Okur, D.V. and Ansal, A. (2007), "Stiffness degradation of natural fine grained soils during cyclic loading", *Soil Dyn. Earthq. Eng.*, **27**(9), 843-854.
- Polito, C.P. and Martin, J.R. II (2001), "Effects of nonplastic fines on the liquefaction resistance of sands", *J. Geotech. Geoenviron. Eng., ASCE*, **127**(5), 408-415.
- Seed, H.B. and Idriss, I.M. (1970), "Soil moduli and damping ratio factors for dynamic response analysis", *Report No. EERC 70-10*, Earthquake Engineering Research Center, University of California, Berkeley, CA, USA.
- Seed, H.B., Idriss, I.M. and Arango, I. (1983), "Evaluation of liquefaction potential using field performance data", *J. Geotech. Geoenviron. Eng., ASCE*, **109**(3), 458-482.
- Tokimatsu, K., Kojima, H., Kuwayama, S., Abe, A. and Midorikawa, S. (1994), "Liquefaction-induced

- damage to building in 1990 Luzon Earthquake”, *J. Geotech. Eng., ASCE*, **120**(2), 290-306.
- Thevanayagam, S. (1998), “Effect of fines and confining stress on undrained shear strength of silty sand”, *J. Geotech. Geoenviron. Eng., ASCE*, **124**(6), 479-491.
- Thevanayagam, S., Ravisbankar, K. and Mohan, S. (1996), “Steady state strength, relative density and fines content relationship for sands”, *Transportation Research Record: J. Transport. Res. Board*, 1547/1996, pp. 61-67.
- Thian, S.Y. and Lee, C.Y. (2011), “Undrained response of mining sand and fines contents”, *Int. J. Civil Struct. Eng.*, **1**(4), 844-851.
- Tsuchida, H. (1970), “Prediction and countermeasure against the liquefaction in sand deposits”, *Abstract of the Seminar in the Port and Harbor Research Institute*, Japan, 3.1-3.33.
- Vaid, V.P. (1994), “Liquefaction of silty soils”, *Ground Fail. Under Seismic Condit., Geotech. Spec. Pub. No. 44*, ASCE, New York, USA, 1-16.
- Wood, D.M. (1991), *Soil Behaviour and Critical State Soil Mechanics*, Cambridge University Press, 40 West 20th Street, New York, NY, USA.
- Xenaki, V.C. and Athanasopoulos, G.A. (2003), “Liquefaction resistance of sand-silt mixtures: an experimental investigation of effect of fines”, *Soil Dyn. Earthq. Eng.*, **23**(3), 183-194.
- Yamamuro, J.A. and Lade, P.V. (1997), “Static liquefaction of very loose sands”, *Can. Geotech. J.*, **34**(6), 905-917.
- Zlatovic, S. and Ishihara, K. (1995), “On the influence of non fines on residual strength”, *Proceedings of the 1st International Conference of Earthquake Geotechnical Engineering (ISTOKYO' 95)*, Rotterdam, The Netherlands, (K. Ishihara and A.A. Balkema Eds.), pp. 239-244.
- Zlatovic, S. and Ishihara, K. (1997), “Normalized behavior of very loose nonplastic soil: Effects of fabric”, *Soil. Found.*, **37**(4), 47-56.